Table 3. Input parameters for example physical models of 182-413

Stellar spectrum:	$T_* = 39\,000$ K
(Simón-Díaz et al. 2006)	$\log g = 4.1$
	$L_* = 2.04 \times 10^5\ L_\odot$
Ionizing flux at proplyd:	$\Phi_H = 1.27 \times 10^{12}$ cm^{-2} s^{-1}
Ionization front radius:	$r_0 = 3.7 \times 10^{15}$ cm
Gas-phase abundances:	Model A: Esteban et al. (2004)
	Model B: this paper
Dust composition:	Standard Orion (Baldwin et al. 1991)

4 PHOTOEVAPORATION MODELS OF HST 10

We have calculated dynamic photoevaporation models of HST 10, using the procedure outlined in § 6 of Mesa-Delgado et al. (2012). The parameters for the models are shown in Table 3. As compared with 177-341 (HST 1), which was modeled in Mesa-Delgado et al. (2012), HST 10 receives a roughly ten times smaller ionizing flux and is roughly twice as large. Since $F \propto n^2 r$ for recombination-dominated photoevaporation flows (Bertoldi & McKee 1990; Henney 2001), this implies that the densities in HST 10 should be $\simeq 5$ times smaller and the ionization parameter $\simeq 2$ times smaller than in HST 1.

Two different abundance sets were used in the models. The first (Model A) is the standard Orion gas phase abundance set, as determined by Esteban et al. (2004). The second (Model B) is the set of abundances determined in this paper by empirical means, see Table 3. The resultant spectrum is shown in Figure 8 for the two cases. It can be seen that the Esteban et al. abundances produce very large discrepancies between the observed and predicted line fluxes (panel a). In particular, all Sulfur, Argon and Chlorine lines are too strong in the model by a factor of 3 to 10, whereas, [O III] 4363 Å is too weak, indicating that the model temperature is too low in the highly ionized regions. On the other hand, the [N II] lines are well-reproduced y this model.

The situation is much improved by using the Model B abundances (panel b), although serious discrepancies remain. The sulfur line fluxes are now in good agreement with the observations, with the notable exception of the [S II] 4070 Å auroral line, which is still 3 times too strong in the model. The [O I] 6300 Å shows a similar behaviour, being too strong by a factor of 4. These two lines, together with the [N II] 5755 Å auroral line, show the strongest contrast between the proplyd and the background nebula, and hence are measured with a relatively small uncertainty, making the disagreement highly significant. The [N II] lines do not agree with Model B so well as they do with Model A, but the agreement is still fair given the uncertainties. The remaining disagreement is with the [N I] 5199 Å line, but this is to be expected since the line arises through fluorescence in neutral gas (Ferland et al. 2012), whereas the model extends only to a hydrogen ionization fraction of 0.1 and therefore misses part of the [N I]-emitting zone.

It is not particularly surprising that the empirically determined abundances do not reproduce the observed fluxes when used in our physical proplyd model. The same was seen in the case of HST 1, where it was argued that the strong gradients in temperature and density, both with and between ionization zones, invalidated the empirical one-zone or two-zone approaches for analysing the spectrum. However, in that case it was possible to find a different set of abundances for the model that succeded in reproducing the observed spectrum to a high precision. Unfortunately, we have been unable to find such a satisfactory model for HST 10. Initial attempts to adjust the abundances have resulted in models that fit the observations *worse* than Model B does.

The two most discrepant lines, [O I] 6300 Å and [S II] 4070 Å have a considerable overlap in their zones of emission. All the [O I] emission, and roughly half of the [S II] 4070 Å arises from partially ionizes gas at the ionization front itself. If the temperature of this gas is overestimated in the models, then the discrepancy could be explained. With the standard Orion dust properties that we are using in all the models (Baldwin et al. 1991), photoelectric emission from dust grains provides up to 15% of the heating in this zone. Since there is some evidence that dust is depleted in the proplyd flows (García-Arredondo et al. 2001), it may be feasible to reduce this heating, which is an avenue that will be explored in future work.

5 SPATIAL VARIATION

The emissivity structure shown in the middle panel of Figure 9 can be compared with the emission line maps presented in § 3.1. The model predicts that the lower ionization lines, such as those of [O I], [S II], and [N II], should show emission that is offset towards the center of the proplyd with respect to the Hα emission by 1–2×10^{15} cm (0.5–1 spaxel), which is very similar to what is observed (Fig. 3). In contrast, the highest ionization lines, such as those of [O III] and [Ne III], should be offset away from the center of the proplyd by a similar amount, which is again consistent with the observed spatial distributions (Fig. 4). The model also makes more detailed predictions about the emission distributions, such as the fact that for both [O III] and [N II] the nebular collisional lines should be weighted towards slightly larger radii than the auroral line, a consequence of the temperature and density gradients within a given ionization zone. There is some evidence for this from our emission maps, but the predicted magnitude of the effect (0.1–0.5 spaxel) is at the limit of what can be discerned with our spatial resolution.

4.3 Comparison with other proplyds

HST 10 is the third proplyd to be subject to a detailed abundance analysis, following earlier studies of LV 2 (Tsamis et al. 2011; Tsamis & Walsh 2011) and HST 1 (Mesa-Delgado et al. 2012). These proplyds cover a broad range in size and in separation from the Trapezium stars (see Figure 10), and derived physical parameters for the three proplyds are summarised in Table 3. HST 10 shows a significantly lower ionization parameter than the two closer-in proplyds, which is reflected in its emission line spectrum that is relatively stronger in low ionization lines. Despite these differences, the estimated mass loss rate from the ionized cusp is very similar for all three proplyds, being of order $2 \times 10^{-7}\ M_\odot$ yr^{-1}. These values are somewhat lower than earlier estimates (e.g., Henney & O'Dell 1999; Henney et al. 2002), which is partly because we are neglecting the contribution of mass loss though the proplyd tail.

Table 4 also shows estimates for the mass and radius of the embedded circumstellar accretion disk, which is the reservoir of mass in the proplyds. All three proplyds show very similar sub-mm fluxes (Mann & Williams 2010), of order 20 mJy once the contribution from ionized free-free emission has been subtracted. However, conversion of this flux to a gas mass requires knowledge of the dust opacity per unit gas mass and dust temperature, both of which have large uncertainties (Williams & Cieza 2011). The values in the table are calculated on the assumption that the dust temperature is the effective temperature of a disk in radiative equilibrium with the

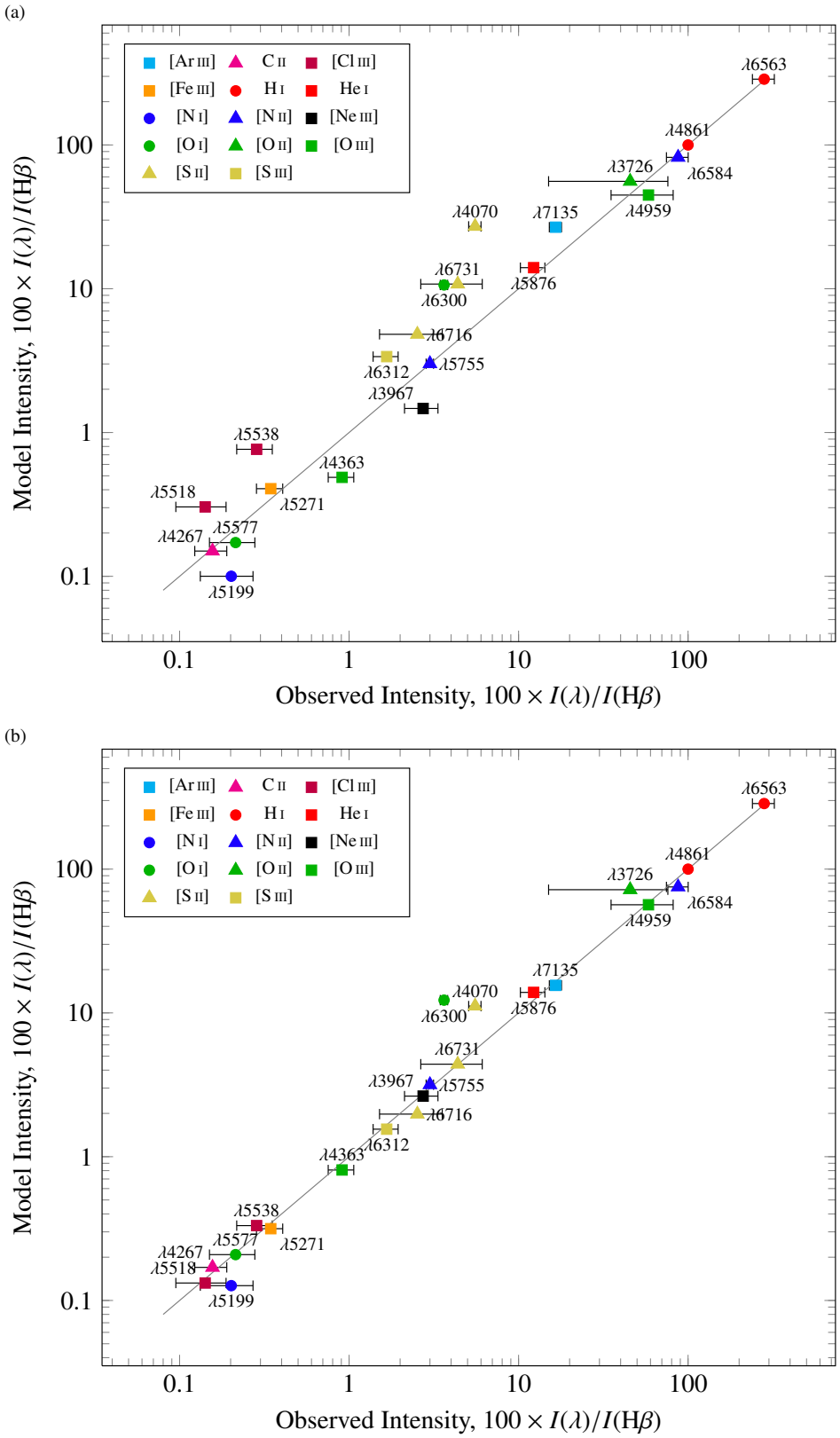

Figure 8. Comparison between predicted and observed emission line fluxes for photoevaporation models of HST 10 with (a) abundances as determined for the Orion Nebula by Esteban et al. (2004), (b) abundances determined for HST 10 in this paper. The agreement in panel (b) is much better, but there are still notable discrepancies.

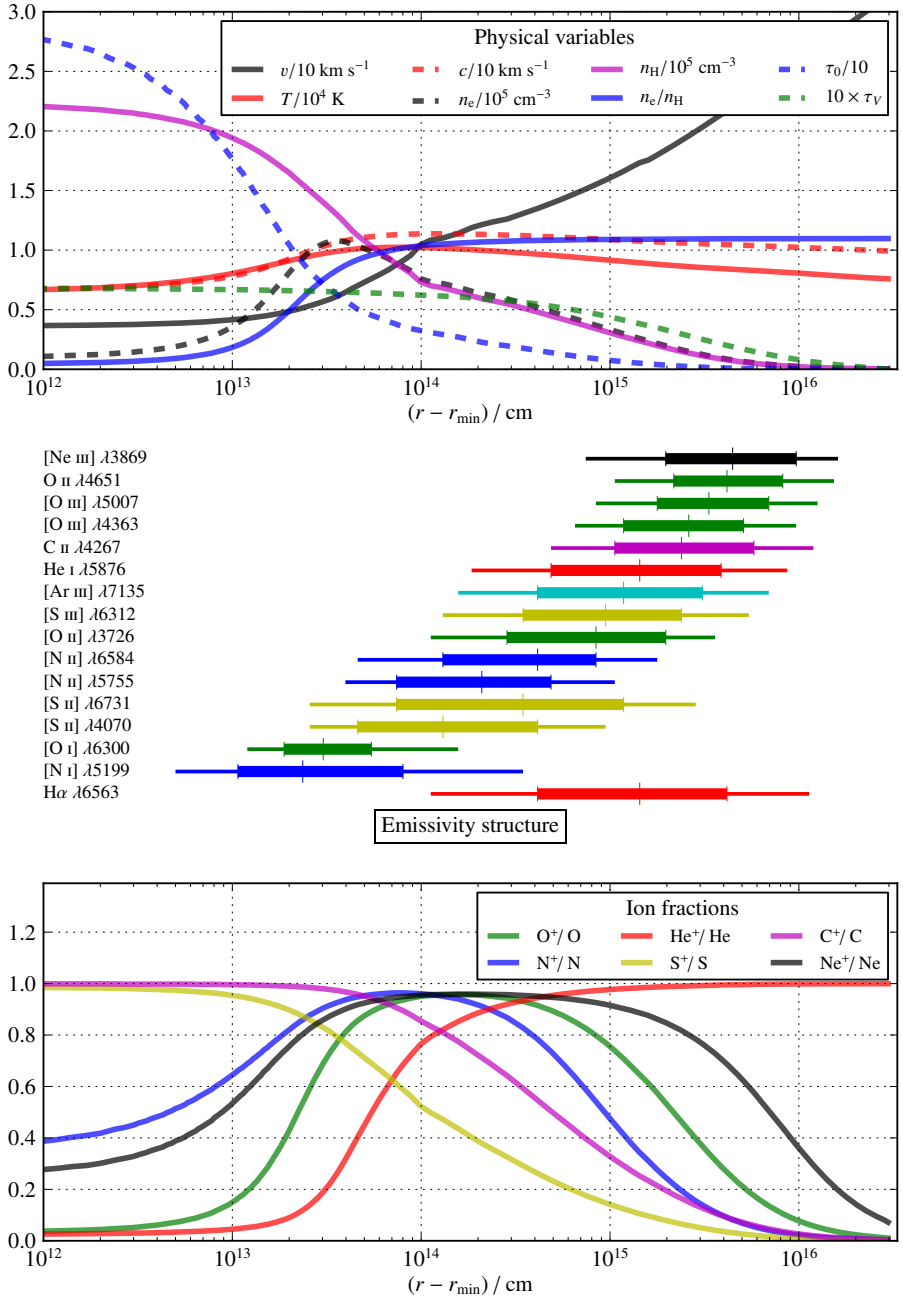

Figure 9. Model structure as a function of radius along a line at an angle of $\theta = 30°$ to the symmetry axis for our photoevaporation Model B. The radius r is measured from the center of curvature of the ionization front, shown on a logarithmic scale with respect to the deepest point in the model, $r_{min} = 3.5 \times 10^{15}$ cm. *Upper panel*: Physical variables. Gas velocity, v, in units of 10 km s^{-1} (solid black line). Gas temperature, T, in units of 10^4 K (solid red line). Isothermal sound speed, c, in units of 10 km s^{-1} (dashed red line). Electron density, n_e, in units of 7×10^4 cm^{-3} (dashed black line). Total hydrogen density, n_H, in units of 7×10^4 cm^{-3} (solid purple line). Electron fraction, n_e/n_H (solid blue line). Lyman limit optical depth, τ_0 (divided by 10), measured from the ionizing source, which is located off the graph at $r = 6.32 \times 10^{17}$ cm (dashed blue line). Visual dust extinction optical depth, τ_V (times 10). *Middle panel*: Emissivity structure for selected emission lines. For each emission line, the vertical line indicates the median emission radius (for which half the total line flux is emitted from gas at smaller radii and half from gas at larger radii), while the thick horizontal bar shows the range between the 25th and 75th quartiles of the emission, and the thin horizontal bar shows the range between the 10th and 90th quartiles of the emission. *Lower panel*: Ionization structure. The fraction of singly ionized ions for a selection of elements is shown by differently colored lines, as indicated in the key. Results for other angles and abundance sets are similar, except with densities that scale roughly as $\cos^{1/2}\theta$, and temperatures that tend to decrease slightly with θ and with increased metal abundances.

Table 4. Comparison of physical properties between HST 10 and two other well-studied proplyds

	Units	Note	LV 2	HST 1	HST 10
Coordinate-based designation		1	167-317	177-341	182-413
Relation to ionizing source					
Projected distance, D'	$''$	2	7.83	25.84	56.7
Inclination, i	$^\circ$	3	50	70	150
True distance, D	pc	4	0.022	0.059	0.242
Ionized cusp					
Ionization front radius, r_0	AU	5	53.	136.	247.
Peak electron density, n_0	10^6 cm^{-3}	6	2.0	0.4	0.1
Ionization parameter		7	0.012	0.008	0.002
Cusp mass-loss rate, $\dot{M}$	10^{-7} $M_\odot$ yr^{-1}	8	2.6	2.5	2.1
Molecular disc					
Disc effective temperature: T_d	K	9	95	58	29
Disc mass M_d	10^{-3} $M_\odot$	10	1.6	2.7	5.4
Disc radius R_d	AU	11	34	89	160
Evaporation time, t_{evap}	10^4 yr	12	0.6	1.1	2.6

Notes: (1) O'Dell & Wen (1994) (2) Angular separation from θ^1 Ori C (O'Dell 1998) (3) Inclination of proplyd axis to line of sight estimated from kinematic studies of the velocity–ionization correlation in emission lines from the cusp (Henney & O'Dell 1999; Henney et al. 2002). Proplyds with $i > 90^\circ$ have their head pointing away from the observer. (4) $D = D'/\sin i$. (5) Estimated from fitting evaporation models to the Hα profiles of the cusps Henney & Arthur (1998). (6) LV 2 from [C III] density (Henney et al. 2002); HST 1 and HST 10 from model fitting (this paper and Mesa-Delgado et al. 2012). (7) $F/(n_0\,c)$. (8) Calculated by integrating model mass fluxes over the area of the cusp. (9) Radiative equilibrium temperature, assuming that 25% of the bolometric flux from θ^1 Ori C reaches the surface of the disk (see also Robberto et al. 2002). (10) Estimated from observed fluxes at 880 μm (Mann & Williams 2010) after subtracting the contribution from ionized free-free emission, assuming optically thin dust emission with opacity $\kappa_\nu = 0.034$ cm^2 g^{-1} and dust temperature equal to the effective temperatures derived above. (11) Directly estimated from *HST* images from HST 10. For LV 2 and HST 1, we assume $r_d = 0.65 r_0$, see Figure 10. (12) Nominal mass loss timescale: $M_d/\dot{M}$.

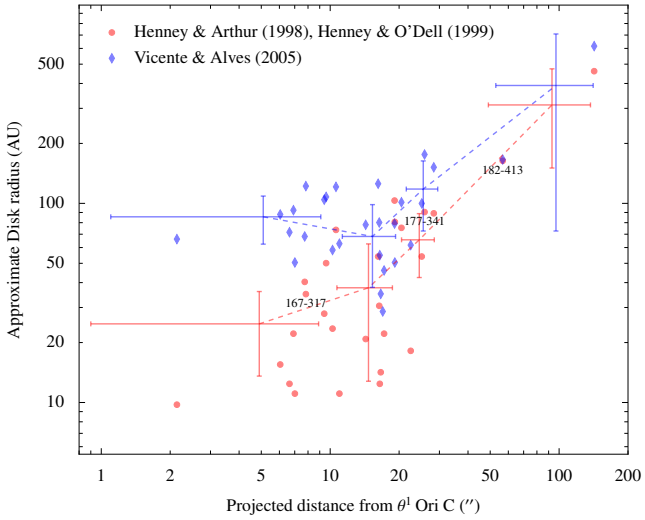

Figure 10. Variation with projected distance from the ionizing star of circumstellar disc sizes in the Orion proplyds. Blue symbols show empirical determinations from Vicente & Alves (2005), red symbols show results from fitting photoevaporation models (Henney & Arthur 1998; Henney & O'Dell 1999). The three proplyds that have been subject to gas-phase abundance studies are marked: 167-317 (LV 2), 177-341 (HST 1), a 182-413 (HST 10). In only a few cases, such as HST 10, is the molecular disc size directly measured, for the rest it is assumed to be half the size of the ionization front. Note that the Vicente & Alves methodology significantly overestimates the true size of the ionization front (and by extension the enclosed disc) for proplyds that are much brighter than surrounding nebula, which tend to be those found close to the ionizing star. Error bars show the mean and standard deviation measured in 4 broad spatial bins.

bolometric flux from the Trapezium stars,[1] and using the opacity recommended by (Beckwith et al. 1990) of $0.1(\nu/1000\ \mathrm{GHz})$ cm^2 g^{-1}, giving 0.034 cm^2 g^{-1} at 880 μm. It must be emphasised that the derived masses are highly uncertain, since the opacity could be up to 20 times smaller if substantial grain growth up to cm-sized bodies has occured (D'Alessio et al. 2001). Evidence for grain evolution has been found in the case of silhouette disks projected onto the Orion Nebula (Miotello et al. 2012). The masses given in the table are at least 6 times smaller than the "minimum mass solar nebula" (Weidenschilling 1977), which is the mass within 30 AU required to account for the composition of the planets in the Solar System.

The nominal photoevaporation timescales, $t_{evap} = M_d/\dot{M}$, are uncomfortably short compared with the estimated age of the photoionized nebula ($\geqslant 10^5$ yr; see discussion in § 8.2.2 of Henney & O'Dell 1999), but would come into agreement if the masses were increased by a factor of 5–10, which cannot be ruled out (see previous paragraph). Interestingly, the evaporation timescale t_{evap} *increases* with increasing distance from the Trapezium. Given that t_{evap} should be roughly equal to the elapsed time since the disk photoevaporation commenced (Johnstone et al. 1998), this is the opposite of what would be expected from a naive model of a roughly spherical H II region, in which case proplyds at greater distances from the ionizing star would have entered the H II region more recently. However, evidence from both observations (O'Dell et al. 2009) and numerical

[1] Although the sub-mm emission is optically thin, the disks are likely to be optically thick at mid-infrared wavelengths where they emit the bulk of their radiation. We assume that 50% of the bolometric radiation from the Trapezium stars is absorbed in the ionized cusp of the proplyd, and that 50% of the remainder is absorbed in the neutral photoevaporation flow, so that only 25% reaches the surface of the disk.

simulations (Arthur et al. 2011) point to the continued survival of dense clumps of molecular gas well inside the apparent boundary of the H II region, in which case it is reasonable that the proplyds closest to the Trapezium might have been shielded from ultraviolet radiation until relatively recently.

The abundance results for the three proplyds are rather disparate, so that it is very hard to see any consistent trend in the results. For instance, although we find a roughly solar oxygen abundance for HST 10 from both empirical analysis and photoevaporation model fitting, the oxygen abundance was found to be $\simeq 3\times$ super-solar in LV 2 (Tsamis et al. 2011) from a purely empirical analysis, with no discrepancy between collisional and recombination lines. In contrast, Mesa-Delgado et al. (2012) found oxygen to be $\simeq 3\times$ *sub*-solar in HST 1, both from empirical analysis of CELs and from photoevaporation model fitting, whereas an empirical analysis of ORLs is more consistent with a solar value. Given the wide range of characteristic ionization and density found in the three proplyds (Table 4), it is possible that systematic errors in our abundance analysis might be contributing to this wide spread. In order to rule out any such effects, it is vital to carry out a similar analysis on a sample of proplyds that all have *similar* ionization parameters and densities.

REFERENCES

Arthur S. J., Henney W. J., Mellema G., de Colle F., Vázquez-Semadeni E., 2011, MNRAS, 414, 1747
Baldwin J. A., Ferland G. J., Martin P. G., Corbin M. R., Cota S. A., Peterson B. M., Slettebak A., 1991, ApJ, 374, 580
Beckwith S. V. W., Sargent A. I., Chini R. S., Guesten R., 1990, AJ, 99, 924
Bertoldi F., McKee C. F., 1990, ApJ, 354, 529
D'Alessio P., Calvet N., Hartmann L., 2001, ApJ, 553, 321
Esteban C., Peimbert M., García-Rojas J., Ruiz M. T., Peimbert A., Rodríguez M., 2004, MNRAS, 355, 229
Ferland G. J., Henney W. J., O'Dell C. R., Porter R. L., van Hoof P. A. M., Williams R. J. R., 2012, ApJ, 757, 79
García-Arredondo F., Henney W. J., Arthur S. J., 2001, ApJ, 561, 830
Henney W. J., 2001, in Revista Mexicana de Astronomia y Astrofisica Conference Series, Vol. 10, Revista Mexicana de Astronomia y Astrofisica Conference Series, Cantó J., Rodríguez L. F., eds., pp. 57–60
Henney W. J., Arthur S. J., 1998, AJ, 116, 322
Henney W. J., O'Dell C. R., 1999, AJ, 118, 2350
Henney W. J., O'Dell C. R., Meaburn J., Garrington S. T., López J. A., 2002, ApJ, 566, 315
Johnstone D., Hollenbach D., Bally J., 1998, ApJ, 499, 758
Mann R. K., Williams J. P., 2010, ApJ, 725, 430
Mesa-Delgado A., Núñez-Díaz M., Esteban C., García-Rojas J., Flores-Fajardo N., López-Martín L., Tsamis Y. G., Henney W. J., 2012, MNRAS, 426, 614
Miotello A., Robberto M., Potenza M. A. C., Ricci L., 2012, ApJ, 757, 78
O'Dell C. R., 1998, AJ, 115, 263
O'Dell C. R., Henney W. J., Abel N. P., Ferland G. J., Arthur S. J., 2009, AJ, 137, 367
O'Dell C. R., Wen Z., 1994, ApJ, 436, 194
Robberto M., Beckwith S. V. W., Panagia N., 2002, ApJ, 578, 897
Simón-Díaz S., Herrero A., Esteban C., Najarro F., 2006, A&A, 448, 351
Tsamis Y. G., Walsh J. R., 2011, MNRAS, 417, 2072
Tsamis Y. G., Walsh J. R., Vílchez J. M., Péquignot D., 2011, MNRAS, 412, 1367
Vicente S. M., Alves J., 2005, A&A, 441, 195
Weidenschilling S. J., 1977, Ap&SS, 51, 153
Williams J. P., Cieza L. A., 2011, ARA&A, 49, 67